

Article

Object-Based Informal Settlement Mapping in Google Earth Engine Using the Integration of Sentinel-1, Sentinel-2, and PlanetScope Satellite Data

Dadirai Matarira ¹, Onesimo Mutanga ² , Maheshvari Naidu ³  and Marco Vizzari ^{4,*} 

¹ School of Agriculture, Earth and Environmental Science, University of KwaZulu-Natal, P/Bag X01, Scottsville, Pietermaritzburg 3209, South Africa

² Department of Geography, University of KwaZulu-Natal, P/Bag X01, Scottsville, Pietermaritzburg 3209, South Africa

³ Department of Humanities, School of Social Sciences, University of KwaZulu-Natal, Durban 4041, South Africa

⁴ Department of Agricultural, Food and Environmental Sciences, University of Perugia, 06121 Perugia, Italy

* Correspondence: marco.vizzari@unipg.it; Tel.: +39-075-585-6059

Abstract: Mapping informal settlements' diverse morphological patterns remains intricate due to the unavailability and huge costs of high-resolution data, as well as the spatial heterogeneity of urban environments. The accessibility to high-spatial-resolution PlanetScope imagery, coupled with the convenience of simple non-iterative clustering (SNIC) algorithm within the Google Earth Engine (GEE), presents the potential for Geographic Object-Based Image Analysis (GEOBIA) to map the spatial morphology of deprivation pockets in a complex built-up environment of Durban. Such advances in multi-sensor satellite image inventories on GEE also afford the possibility to integrate data from sensors with different spectral characteristics and spatial resolutions for effective abstraction of informal settlement diversity. The main objective is to exploit Sentinel-1 radar data, Sentinel-2 and PlanetScope optical data fusion for more accurate and precise localization of informal settlements using GEOBIA, within GEE. The findings reveal that the Random Forests classification model achieved informal settlement identification accuracy of 87% (F-score) and overall accuracy of 96%. An assessment of agreement between observed informal settlement extents and ground truth dimensions was conducted through regression analysis, yielding root mean square log error (RMSLE) = 0.69 and mean absolute percent error (MAPE) = 0.28. The results demonstrate reliability of the classification model in capturing variability of spatial characteristics of informal settlements. The research findings confirm efficacy of combined advantages of GEOBIA within GEE, and integrated datasets for more precise capturing of characteristic morphologic informal settlement features. The outcomes suggest a shift from standard static conventional approaches towards more dynamic, on-demand informal settlement mapping through cloud computing, a powerful analysis platform that simplifies access to and the processing of voluminous data. The study has important implications for identifying the most effective ways to map informal settlements in a complex urban landscape, thus providing a benchmark for other regions with significant landscape heterogeneity.

Keywords: Google Earth Engine; simple non-iterative clustering; object-based image analysis; informal settlements; texture features; mapping



Citation: Matarira, D.; Mutanga, O.; Naidu, M.; Vizzari, M. Object-Based Informal Settlement Mapping in Google Earth Engine Using the Integration of Sentinel-1, Sentinel-2, and PlanetScope Satellite Data. *Land* **2023**, *12*, 99. <https://doi.org/10.3390/land12010099>

Academic Editors: Tomasz Noszczyk and Abreham Berta Aneseyee

Received: 23 November 2022

Revised: 24 December 2022

Accepted: 25 December 2022

Published: 28 December 2022



Copyright: © 2022 by the authors. Licensee MDPI, Basel, Switzerland. This article is an open access article distributed under the terms and conditions of the Creative Commons Attribution (CC BY) license (<https://creativecommons.org/licenses/by/4.0/>).

1. Introduction

Unprecedented processes of urbanization, especially in countries of the global south, result in highly dynamic urban patterns, characterized by dominance of informal urban development [1]. Being inexorably a reflection of the “urbanization of poverty” [2], informal settlements are characterized by dense housing, made up of sub-standard, heterogeneous

construction materials, which, when coupled with their characteristic location on flood-vulnerable areas, exacerbate residents' risk and vulnerability to natural hazards such as flood events [3]. With this type of housing playing host to approximately one billion dwellers globally [4], the United Nations has prioritized informal settlement improvements in the 2030 Sustainable Development Goals [5,6]. However, despite these stipulated targets, informal settlements continue to grow [6]. Ameliorating the conditions of deprivation in informal settlements requires up-to-date base maps with comprehensive information on their spatial locations and dimensions [3], which is mostly inconsistent, generalized or simply non-existent [7]. Given the dynamic nature of these deprived areas [8], there is an exigency for techniques that can provide rapid and reliable information on their morphological layouts. To this end, Belenok et al. [9] have noted a need for the constant improvement of methods that assess the current state of cities' anthropogenic landscapes in view of potential environmental urbanization consequences. In light of this, the understanding of informal settlements' levels of marginalization, as they relate to natural hazards and climate change risk, requires precise and comprehensive identification of their spatiality.

Remote sensing provides ease of spatial analytics [10], and its synoptic and repetitive capabilities afford updated, consistent and comprehensive geospatial information with great thematic detail, especially in complex urban environments [11]. Exploiting the convenience of high-resolution sensors such as GeoEye, IKONOS, QuickBird and WorldView, concerted research efforts have been made to map informal settlements [12–15]. However, the intricacy of the semantic abstraction of informal settlements has been emphasized [16–18]. Firstly, the cost-prohibitive nature and, sometimes, unavailability of high-resolution earth observation (EO) data [7] is a major drawback in promoting efforts for the accurate delineation of urban deprived areas. Secondly, the inherent variations in informal settlement morphological appearances, either within or across geographical locations [19], confound the task. Moreover, fragmented urban landscapes are difficult to represent using a pixel-based classification approach where only spectral values are concerned [16], making characterization of informal settlement morphologic differences complex [13,20].

Recently, object-based image analysis (OBIA) or geographic object-based image analysis (GEOBIA) has been applied more frequently in capturing heterogeneity in fragmented urban landscapes for informal settlement identification [5,6,16–18]. The strength of object-oriented approaches (OOA) for informal settlement analysis is in its capability to incorporate spectral, spatial and contextual characteristics of an image, which intensify the potential to capture informal settlement morphological diversities [17,21]. Kohli et al. [17] used OBIA to map informal settlements in Pune, India, using Quickbird imagery, and yielded overall accuracy of 80.8%. In another study, Fallatah et al. [22] mapped informal settlements in Jeddah, Saudi Arabia, and distinguished informal and formal areas with an overall accuracy of 83%. In a further progression of this work, taking advantage of machine learning, they synergistically combined with OBIA to improve informal settlement mapping in Saudi Arabia, achieving enhanced overall accuracy of 91% from GeoEye-1 imagery [16]. An attempt to integrate data from two sensors for OBIA was presented by Pratomo et al. [5], combining GeoEye-1 and Landsat data in the Middle Eastern environment, achieving overall Random Forests (RF) classification accuracy of 95%. These past efforts focused on the ontological framework suggested by Kohli et al. [23] using a range of informal settlement indicators for segmentation at different scale levels. In that regard, Fallatah et al. [22] reported the need for expert knowledge in transferring informal settlement indicators into local knowledge. In addition, the popularly used eCognition software, for segmentation, requires a high level of image analysis skill in translating such indicators into informal settlement identification [22]. In addition, the framework involves different levels of rigorous segmentation as well as numerous processing steps for the classification refinement at different spatial levels [18]. Sometimes, segmentation and classification are performed in two different software [16]. Fallatah et al. [16] described the whole process as time-consuming and cumbersome. In fact, numerous processing steps enforce a weighty computational and storage burden on local computation platforms.

Google Earth Engine (GEE), with its engrained segmentation algorithms, has presented potential solutions to long-standing challenges of complex segmentation and classification steps encountered when using classical image processing softwares. Access to advanced algorithms that are highly parallelized behind the scenes [24] presents ease of analysis and classification, as well as for visualization of outputs [25]. Apart from being a powerful platform for image collection and organisation [26], GEE provides an application program interface for summoning, processing, and stacking image input data, running all analyses in parallel [27]. Within GEE, three segmentation algorithms can be implemented, which include K-means, G-means, and Simple Non-Iterative Clustering (SNIC) [28]. According to Achanta and Susstrunk [29], SNIC is computationally cheaper and uses less memory than the K-means and G-means. The feasibility of the SNIC algorithm for object-based mapping applications has been investigated [25,30–32]. SNIC has been successfully employed for Land Use/Land Cover (LULC) mapping using PlanetScope (PL), Sentinel-2 (S2), and Sentinel-1 (S1) data in central Brazil [32], for winter wheat mapping, using S2 in China [28] and for crop mapping in China, using S1 data [30]. Significant improvements in mapping accuracy have also been reported when the OBIA approach was integrated with Grey Level Co-occurrence Matrix (GLCM) texture features within GEE [25,32–34]. The GLCM algorithm permits the calculation of image textural indices based on second-order statistics for image texture analysis [35]. According to Kohli et al. [21], a texture analysis approach is critical in discriminating between formal and informal areas, which are sometimes difficult to distinguish using the OBIA technique.

The advent of GEE has also increased data accessibility through the engrained abundant imagery archives, for example S1 and S2, Landsat and MODIS [36]. Of late, the availability of high resolution PL data within GEE has made OBIA implementable in the mapping of heterogeneous terrestrial environments [32]. To take advantage of variations in spectral or spatial domains of sensors available within the GEE platform, GEE presents opportunities for data fusion [37]. Whilst optical sensors, for example S2, are sensitive to the reflectivities of ground targets [38], SAR sensors (e.g., S1) are reactive to their structural, textural, and dielectric characteristics [39]. Amani et al. [40] added that SAR data can provide more differentiable land cover information than multi-spectral data. The synergistic use of different sensors such as S1, S2, and PL EO data has offered opportunities for different mapping applications, especially in highly dynamic, fragmented landscapes. For instance, Mahdianpari et al. [41] integrated S2 and S1 for wetland mapping. Similarly, Tavares et al. [42] combined S2 and S1 for urban LULC mapping in Brazil. Vizzari [32] and Rao et al. [43] compared the performances of PL, S2 and S1 for LULC and crop mapping, respectively. The authors demonstrated the benefits of integrating data from all three sensors, yielding accuracy levels of 91% and 85%, respectively. Research endeavors that incorporated PL imagery reported improved classification of subtle features [32,34,43], presenting opportunities for semantic abstraction of small deprivation pockets, identification of which is inherently difficult [5]. According to Bwangoy et al. [44], classification of multi-source satellite data yields higher classification accuracy relative to the accuracy achieved by a single source data. Supporting the argument, Liu et al. [45] put forward that the integration of two complementary datasets has the potential to minimize classification uncertainty.

Owing to this background, the study sought to integrate data from PL, S2, and S1 and perform GEOBIA, within GEE, to map spatial heterogeneity of morphological informal settlements in a geographically diverse Durban landscape, South Africa. To the best of the authors' knowledge, there has not been any study that has exploited OBIA on PL imagery for capturing structural heterogeneity of informal settlements. Most importantly, GEOBIA, comprising integration of object segmentation and object textural analysis, has not been exploited for informal settlement analysis within the GEE environment.

The main objectives of the study are to: (a) develop an improved, reliable and reproducible object-based classification workflow, within GEE, for capturing high morphological variability in an informal settlement landscape; (b) investigate SNIC based OBIA, within GEE, in accurately capturing subtle deprivation pockets in a heterogeneous landscape; and

(c) exploit the potential of multiple datasets to synergistically enhance semantic abstraction of morphologically diverse areas of deprivation in a fragmented, built-up area of Durban.

2. Materials and Methods

2.1. Study Area

The current research was carried out in part of Durban Metropolis, South Africa (Figure 1). Located in the province of KwaZulu-Natal (Figure 1a), the metropolitan area stretches from between longitudes $30^{\circ}56'30''$ E and $30^{\circ}59'30''$ E, and latitudes $29^{\circ}47'30''$ S and $29^{\circ}50'30''$ S covering area of 1182 ha. According to Williams et al. [46], Durban is characterized by an estimated population of 3.6 million, ranking third in South Africa in terms of population size. The topography of the area is steep and highly undulating, ranging from about 30 m to 120 m above sea level. Most of the informal settlements are located on steep terrain, geometry that contributes to intricacies in capturing uniqueness in a morphologically diverse informal settlement landscape. Generally, Durban is characterized by a humid subtropical climate with mean annual precipitation exceeding 1000 mm per annum [46]. Mild, dry winters and warm, wet summers also characterize Durban. Because of the accommodation crisis, informal settlements present the main form of inadequacy in terms of housing in the city of Durban with, approximately, 75 percent of the metropolitan gross housing backlog of 305,000 units representing informal dwellings [47]. Durban is characterized by varied morphological patterns, ranging from lining traffic arteries, occupying open spaces, to being in proximity to river networks. Most of the roads along which the informal settlements are situated also follow a steep topography and often lead down to Umgeni River, making the residents vulnerable to flood hazards during extreme climatic conditions [48]. Additionally, the characteristic location of the informal settlements on steep slopes, sometimes characterized by fragile soils, contributes to their vulnerability to landslides.

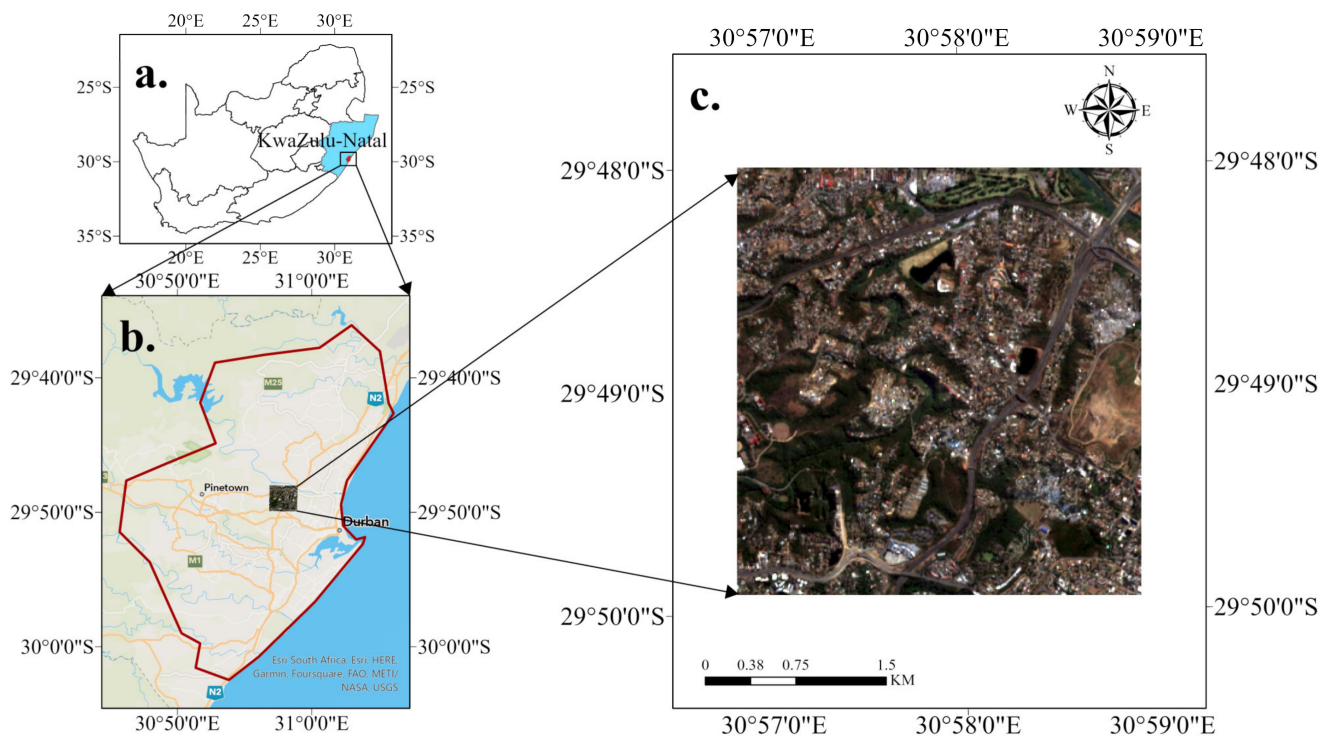


Figure 1. Study area selected in KwaZulu-Natal province (a), within Durban Metropolis (b), South Africa, (c) is the overview of the area obtained with an RGB PlanetScope imagery, in UTM/WGS84 plane coordinate.

2.2. Methodology

The workflow of this approach mainly included image collection, pre-processing, and composition, image segmentation, and texture feature extraction, RF classification, and accuracy assessment (Figure 2). Firstly, PL, S2, and S1 images were collected for the chosen period and study area. Secondly, segmentation of the image into clusters was performed using SNIC algorithm. Thirdly, GLCM algorithm was computed for the calculation of texture metrics. Fourth, object-based classification was performed using RF protocol. The confusion matrix was finally computed for accuracy assessment. The GEE platform was utilized for implementation of all the mentioned procedures.

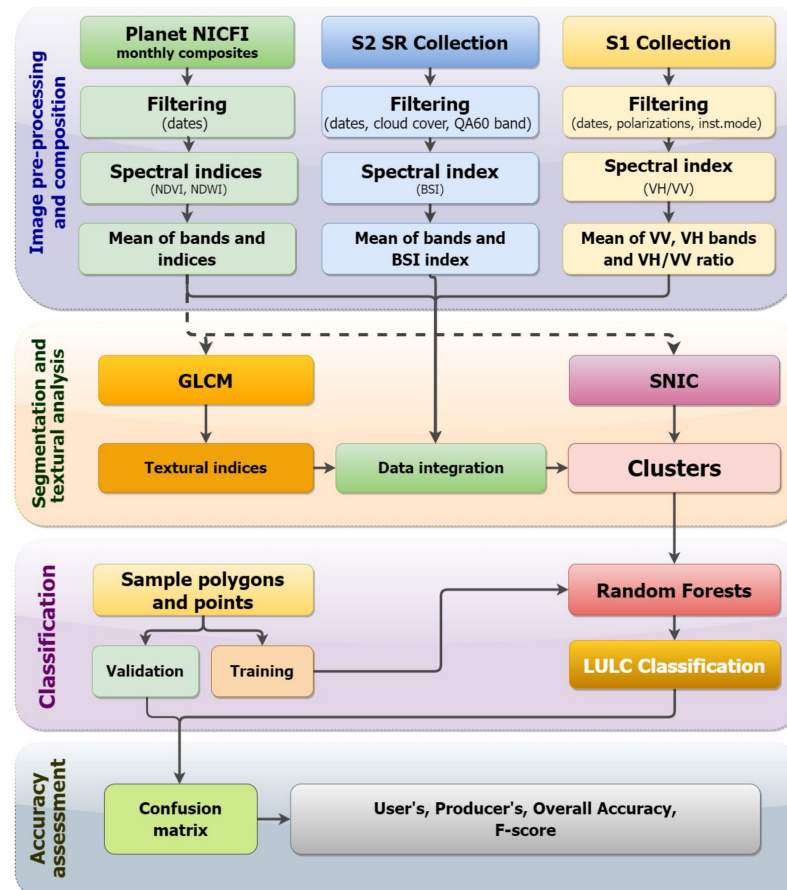


Figure 2. Workflow chart of the methodology.

2.2.1. Data Collection, Pre-Processing, and Image Composition

According to Tassi et al. [33], an important step in LULC classification within GEE is the generation of the base composite dataset. The study utilized data from two optical sensors, PL and S2, and one radar sensor, S1, that fell within the study period (1 June 2021 to 31 December 2021). PL imagery are acquired by 120 CubeSat 3 U satellites measuring $10 \times 10 \times 30$ cm, referred to as a dove [49]. Its sensors can detect 4 spectral bands (RGB and NIR) with a spatial resolution of between 3 and 5 m. The high-resolution composite base maps for PL have recently become accessible in GEE for the tropical regions, appreciations to the partnership between Google and the NICFI (Norway's International Climate and Forest Initiative). In the study period, PL images are available in GEE as cloud-free monthly composite. S2 data, already available in GEE as orthorectified and radio-corrected to provide surface reflectance values, was utilized in the analysis [32,50]. S2 images were filtered considering the cloud coverage of less than 10%. In this step, the study leveraged band QA60 of S2 that signifies the opaque and cirrus clouds to mask cloud cover for S2.

Normalized difference vegetation index (NDVI), and normalized difference water index (NDWI) were computed from PL data, while bare soil index (BSI) [51] was calcu-

lated using S2 data. Being the widely-used index in texture-based informal settlement detection [12,14], NDVI quantifies vegetation cover and better discriminates LULC classes. According to Bouzekri et al. [52], NDWI is the best index for distinguishing road networks, for example tarred roads in formal areas, compared to a mixture of sand, gravel and mud which is characteristic of informal settlements. In addition to capturing brightness of roads, thus, detecting tarred roads with low brightness [16], NDWI also identifies water bodies [50]. The NDVI layer was calculated from the red (B3) and near-infrared (B4) bands of the PL image, whilst NDWI was calculated from the green (B2) and near-infrared (B4) bands of the same satellite. BSI is an index constructed from a combination of the NDVI and the normalised difference built-up index (NDBI) [53]. The index effectively distinguishes bare land from built up land, land cover classes with relatively similar spectral characteristics [54].

S1 carries a single C-band synthetic aperture radar instrument that supports operation in single polarisation (HH or VV) and dual polarisation (HH + HV or VV + VH). The study utilized two diverse polarisation modes which include single co-polarisation with vertical transmit/receive (VV) and dual-band co-polarisation with vertical transmit and horizontal receive (VH). Following Vizzari [32], the ratio between two polarization modes was used to create an additional band, VH_VV. The ratio feature partially compensates for the radiometric instability of the sensor and shows higher stability than the single polarization [55]. The ratio has been proven promising for identifying non-forested wetlands [40]. The mean values were obtained in GEE with a simple “reduce” step for all the PL, S2, and S1 bands and derived indices, thus creating 6-month composite images.

2.2.2. Image Segmentation with SNIC

Segmentation involves splitting an image into objects by clustering neighbouring pixels with similar values [56]. The current study implemented image segmentation within the GEE environment, using the SNIC algorithm. SNIC is an enhanced version of Simple Linear Iterative Clustering algorithm (SLIC) [57] which uses super pixel segmentation to simplify images into small clusters of image-connected pixels [29]. In the current research, SNIC analysis was executed on the visible and NIR (4) bands of PL datasets, segmenting the image into a set of super pixels. Within the GEE platform, SNIC categorizes the objects (clusters) with regard to the set input parameters, visits pixels only once and clusters pixels without iterations [29]. The input parameters include: “image”, “size”, “compactness”, “connectivity”, “neighbourhood size” and “seeds” [30] (see Shafizadeh-Moghadam et al. [25] for definitions). Of these parameters, Shafizadeh-Moghadam et al. [25] iterated that the main ones are “compactness factor”, the “connectivity”, and “neighborhood Size”. Accordingly, after consideration of the characteristics of the landscape patches in the area of study, these parameters were experimentally set as follows: “compactness” = 1, “connectivity” = 8, “neighbourhood Size” = 128. The selection of parameters and parameter values are based on repeated iterations as well as visual evaluation of the outputs [31,33]. SNIC is performed using a regular grid of seeds as input generated by the “Image.Segmentation.seedGrid” function [34] which requires a super pixel seed location spacing (in pixels) for the generation of seed grid. After consideration of the textural characteristics of the landscape patches in the study areas, seed spacing values (5, 10, 15, 20) were also tested iteratively and were then set at 10 for PL. To create the dataset for classification, the mean value of bands contained in the multispectral-textural datasets were computed on an object basis using a “reduce connected component” step. In order to allow visualization of the actual size of the objects, a proper output scale of clusters was fixed using the “reproject” function (scale = 5) [34]. Finally, the algorithm was used to compress the dataset and generate a combined raster made up of clusters and added data layers encompassing the mean values of the input features.

2.2.3. Texture Analysis

In order to improve the image classification and avoid fuzziness, additional contextual information in the form of textural information was computed in GEE using the GLCM algorithm [30,58]. The textural information was extracted only from PL imagery. Following prior studies that have incorporated image texture in OBIA for informal settlement detection [5,16,22,59], contrast, entropy, variance, homogeneity, mean and angular second moment were the texture indices employed in the mapping. The descriptions of the texture metrics are shown in Table 1. GLCM application in GEE requires establishment of a grey level 8-bit image as the input image. As performed in previous studies [34], the grey level image was generated from PL data using the following formula:

$$\text{Grey} = (0.3 \times \text{NIR}) + (0.59 \times \text{RED}) + (0.11 \times \text{GREEN}) \quad (1)$$

Prior application of GLCM, the grey level image was rescaled in the 0–255 range, using the 2nd and the 98th percentile as lower and upper limits [32], in order to improve the results. The window size used in the current study for GLCM was 5×5 , which was established after various testing operations.

Table 1. Texture metrics computed using GLCM.

Code	Texture Features	Textural Index Description
T1	Angular second moment	Describes how uniform the distribution of grey levels is in the image
T2	Contrast	Measures variations in intensity of neighbouring pixel pairs
T3	Mean	Measures the mean of the grey level sum distribution of the image
T4	Entropy	Quantifies the randomness of the grey-level intensity distribution
T5	Variance	Measures how spread out the distribution of grey levels is in the image
T6	Homogeneity	Measures the homogeneity of the image

2.2.4. Object Based Image Classification

Table 2 shows the spectral bands, spectral indices and texture metrics used for the object-based RF classification. The table also presents the sensors from which the variables were derived. Following Vizzari [32], before proceeding to the final band fusion, a bicubic resampling was used to resample S2- and S1-derived layers to a resolution of 5 m. A “reduce connected components” step was performed to calculate the average values of all available bands based on PL-derived SNIC objects. An RF protocol involving 200 trees was implemented on the PL, S2, and S1 composite dataset. The RF approach uses bootstrap sampling technology that selects, at random, a specific number of samples from the original set of training samples to create a new training data set [30]. The choice of the classifier was made owing to its capability to handle urban area classification where dimensional feature spaces are concerned, as well as its robustness for informal settlement detection in complex urban environments [60]. Numerous mapping applications using OBIA within GEE [25,31,42] have shown the superiority of RF in object-based LULC classification. The RF method has the advantages of easy parameterization and robustness against high-dimensional data and overfitting [31], as well as the ability to compute the relative importance of all elements in the classification model [26]. Five land cover types, (i) Informal settlement, (ii) Bare land, (iii) Water, (iv) Other urban, and (v) Vegetation, were used as the classification scheme. Table 3 shows the definitions of the land cover classes. A total of 1750 random sample points were collected and visually classified in QGIS using Google high spatial resolution imagery. Seventy percent of these points were used to train the RF classifier, and the remaining thirty percent to validate the final LULC classification results.

Table 2. The optical, SAR, spectral and textural features applied to the classifications in this study.

Satellite	Band Types	Features
PL	Main channels	B (blue), G (green), R (red), NIR
	Spectral indices	$NDVI = \frac{B4 - B3}{B4 + B3}$, $NDWI = \frac{B2 - B4}{B2 + B4}$
	Textural features	Angular second moment, contrast, variance, homogeneity, mean, entropy
S2	Main channels	B8, B11, B12
	Spectral index	$BSI = \frac{(B12 + B4) - (B8 + B2)}{(B12 + B4) + (B8 + B2)}$
S1	Main channels	VV, VH
	Ratio features	VH-VV

Table 3. The definitions of Land Use/Land Cover classes.

Class	Description
Informal settlement	Densely built housing units that are contiguous
Bare land	Exposed soil with neither grass, trees, nor built-up structures
Water	Water bodies like dams, rivers, ponds, and swamps
Other Urban	Housing units with regular layout pattern, residential, commercial, industrial, freeways, highways, tertiary or local roads
Vegetation	Area covered by grasslands, forests, croplands, small shrubs, sparse and dense trees

2.2.5. Accuracy Assessment

According to Hu et al. [56], assessing the quality of a classified map is crucial for verifying its suitability for the intended purpose and understanding the corresponding map errors. Quantitative analysis of the classification accuracy involved the use of a confusion matrix and its derived accuracy indices, which are overall accuracy (OA) (Equation (2)), producer accuracy (PA) (Equation (3)), user accuracy (UA) (Equation (4)), and F-score measure (Equation (5)), all computed within GEE. According to Zurqani et al. [61], the F-score shows how effective the classifier is in the context of both PA and UA, by weighting their average. F-score is computed as a harmonic mean of PA and UA.

$$OA = \frac{\text{Number of correct predictions}}{\text{Total number of predictions}} \quad (2)$$

$$PA = \frac{\text{Number correctly identified in a given map class}}{\text{Number actually in that reference class}} \quad (3)$$

$$UA = \frac{\text{Number correctly identified in a given map}}{\text{Number claimed to be in that map class}} \quad (4)$$

$$F - \text{score} = 2 \times \frac{(PA * UA)}{(PA + UA)} \quad (5)$$

Further, the study also assessed spatial agreement of the classified outputs with ground truth samples regarding the extent of informal settlements. Seven informal reference settlement samples were identified from the VHR Google Earth Pro image. Malambo and Heatwole [62] demonstrated the reliability of VHR image depiction as an independent source for validation data collection. For the area assessment, polygons for these ground truth samples were digitized, and their areas were measured. Corresponding areas for the classified patches for the same identified samples were also calculated. The statistical evaluation of the correct depiction of spatial extents was carried out using regression analysis in R statistical software, using root mean square log error (RMSLE) and mean absolute percent error (MAPE) accuracy metrics.

2.2.6. Feature Importance Assessment

The current research utilized the RF algorithm for variable importance evaluation. According to Zhao et al. [63], the evaluation of variable importance score entails turning into a number, the contribution of a feature parameter in terms of its impact on the classification accuracy. A variable importance graph was drawn in GEE to show the relevance of all the features used in the classification. This graph supported an iterative selection of the most relevant features in the classification.

3. Results

3.1. Accuracy Assessment of the LULC Map

The LULC object-based classification map using PL, S2, and S1 combined data is presented in Figure 3. The generated LULC map was visually and statistically evaluated using Google Earth Pro imagery and a confusion matrix, respectively. To better display the details, some informal settlement areas were selected from the classified map and compared with their equivalent Google Earth Pro images. Visually, when compared with high-resolution satellite imagery, results of LULC classification indicates that SNIC based object-based classification using integrated data inputs from PL, S2 and S1 delineated informal settlements accurately with satisfactory visual depiction.

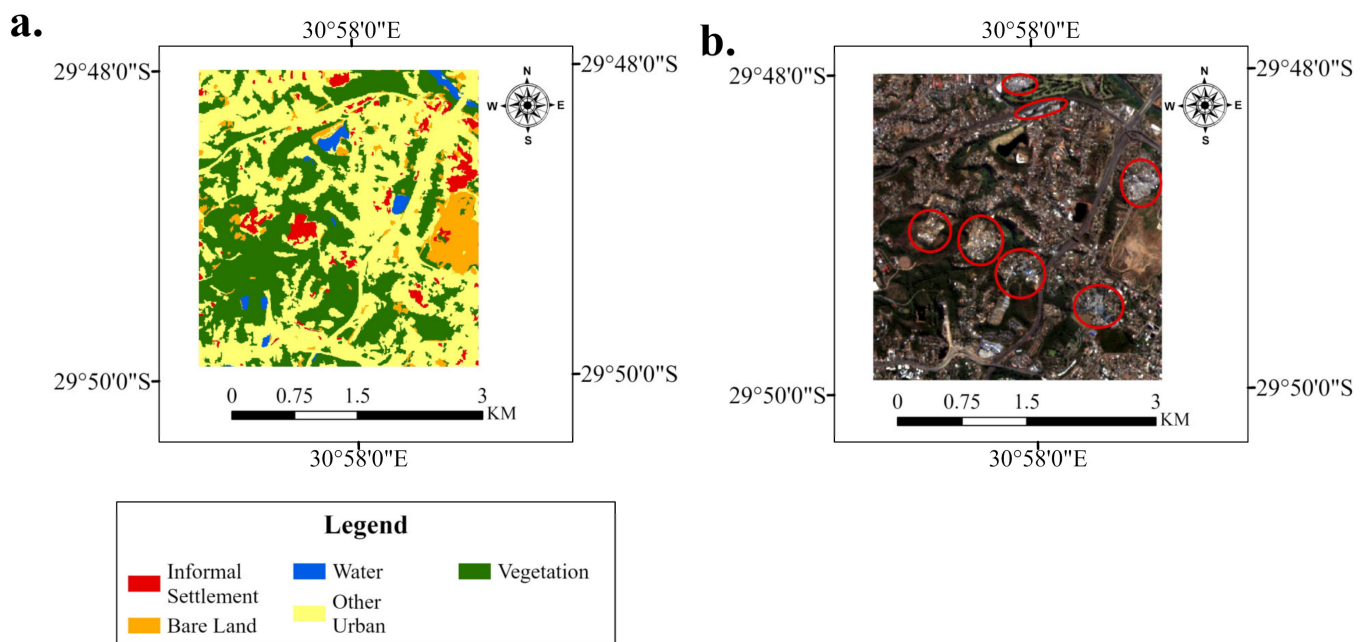


Figure 3. Comparison of results of informal settlements and LULC classification (a) and visual appearance of informal sample settlements on an RGB image (b) (circled in red).

Table 4 shows the accuracy of the classifications obtained from the confusion matrix. The overall accuracy from this experiment is 96%, exceeding 85%, which, according to Kpi-ebaareh et al. [64] is the threshold for a good classification. The class-based performance evaluation revealed that all LULC classes had high F-score values (>85%), indicating that all the classes were clearly identifiable overall using this approach. Informal settlement class yielded an F-score of 87%. However, the informal settlement class registered the lowest F-score, considering results for other LULC classes.

Table 4. Confusion matrix derived from LULC classification. PA: Producer’s Accuracy; UA: User’s Accuracy, and Overall Accuracy in bold.

	Informal Settlements	Bare Land	Water	Other Urban	Vegetation	PA
Informal settlement	44	0	0	10	0	81%
Bare land	1	39	0	1	1	93%
Water	0	0	26	0	0	100%
Other urban	0	0	0	115	0	100%
Vegetation	2	1	0	3	282	98%
UA	94%	98%	100%	89%	100%	96%
F-score	87%	95%	100%	94%	99%	

Figure 4 shows informal settlement patches overlaid on digitized polygons for the same settlement. The results revealed the level of disagreement in spatial extent between the classification output and ground truth samples for informal settlements. Calculations of relative spatial errors demonstrated RMSLE of 0.69 and MAPE of 0.28. The results indicate evidence of underestimation of the spatial extents by the model.

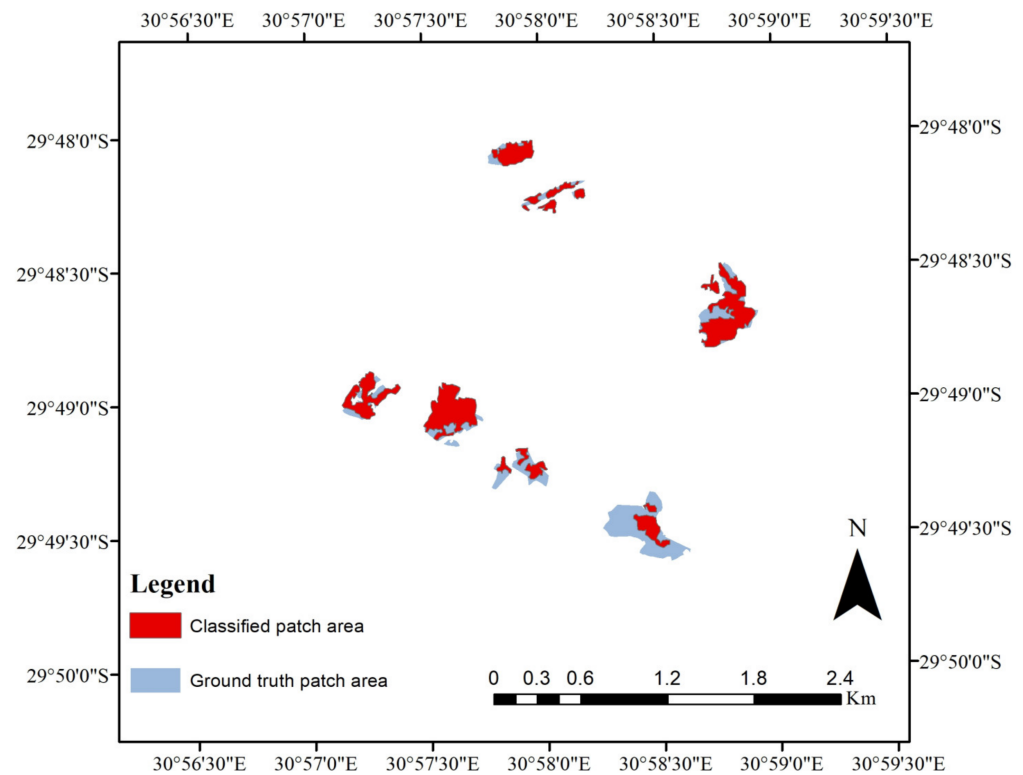


Figure 4. Classified informal settlement patch areas against ground truth patch extents.

3.2. Relative Contribution of Input Variables in RF Classification

Figure 5 shows the relative importance of the different input features in the classification model and the sensors from which the features are derived. The results indicate that S2 band 8 (B8), PL band 1 (B), NDWI, BSI, T5 (homogeneity), and T4 (variance) were the six most important input variables in the classification. Homogeneity was the most important texture variable.

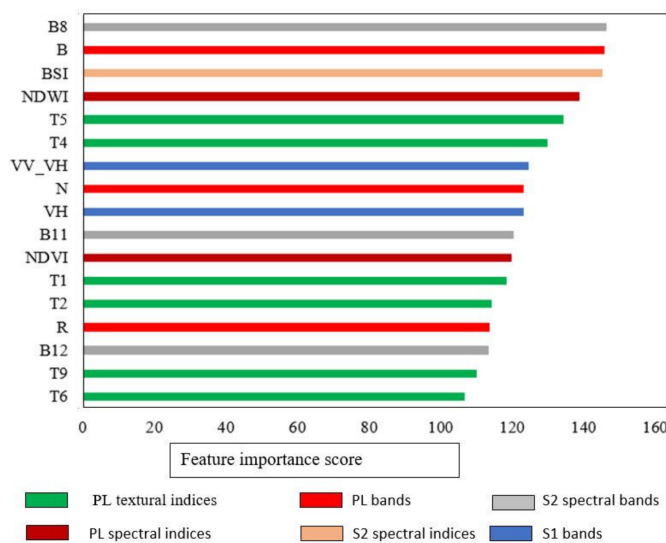


Figure 5. Importance assessment of LULC classification features. Features' codes are reported in Tables 1 and 2.

4. Discussion

The study sought to investigate the capability of object-based image classification, performed within GEE cloud computing environment, for improved mapping of complex informal settlement morphologies. The study capitalized on the embedded SNIC segmentation algorithm, the GLCM algorithm, and the availability of high-resolution PL and Sentinel (S1 and S2) imagery within GEE, to precisely capture informal settlement diversities in a heterogeneous built-up landscape. Versatility of the coding platform available within GEE [65] and good reliability of GEE integrative packages for feature construction, as well as ease of classification process, were explored to allow reproducibility of reliable maps. This study is the first to introduce OBIA in GEE for informal settlement identification.

Generally, the results of the analysis demonstrated that performing OBIA on a 3-sensor dataset within the GEE was successful in accurately depicting all LULC classes in the study area, yielding overall accuracy of 96%. This accuracy value is far above the 85% which, according to Kpienbaareh et al. [64], is a threshold for good classification. Class-specific accuracy results also indicated that all classes were accurately captured with F-score values ranging from 87% to 100%. Such high classification results demonstrate the proficiency of OBIA classification within GEE. An informal settlement identification accuracy (F-score) of 87% demonstrates how an improved workflow within the GEE can generate high-quality informal settlement maps in an area with high morphological variability. The results confirm the proficiency of experimental design and code writing [30] in allowing accurate informal settlement identification. Taking advantage of enfolded SNIC segmentation algorithms and integrated data from PL, S2, and S1, the results confirm the effectiveness of the approach in capturing variability of spatial characteristics of informal settlements in a heterogeneous urban environment of Durban. Mirroring the findings both overall and at class level, the RF model was also able to capture the inner structural heterogeneity in the informal settlement landscape. The worth of RF in mapping complex environments within GEE is emphasized [25,31,32,42]. The current findings concur with previous studies that integrated sensors within GEE in mapping complex environments, for example, crop types [43,64], and LULC in the complex agri-natural space [32]. Their studies suggested the importance of including all the sensors in the classification. Agreeing with the assertion from Bwangoy et al. [44] that multi-source satellite data offer potential for obtaining higher classification accuracy compared to the accuracy achieved by a single source data, Vizzari [32] observed that textural analysis on image objects computed from PL data, and integrated with the spectral information derived from S2 and S1, boosted the efficacy of the 3-sensor dataset combination. The high accuracy levels obtained from

integrating various datasets in the current study are also in agreement with earlier efforts by Fallatah et al. [5], who through the integration of GeoEye data with time-series Landsat data, confirmed the relevance of integrating data from different sensors in informal settlement mapping. Advancing works in Jeddah, Saudi Arabia, yielded overall accuracy levels of 95%, compared to 83% for OBIA alone [22], and 91% for integrated machine learning and OBIA [16]. Similarly, Liu et al. [45] mapped green cover using object-based approach and integrated Unmanned Aerial Vehicle (UAV) multispectral data and light detection and ranging (LiDAR) data. Their results also revealed significantly improved classification accuracy and reduced classification uncertainties in comparison to using either multispectral image or LiDAR data alone.

The suitability of texture parameters in clearly distinguishing built-up areas from other complex classes, especially bare land, has been emphasized [17,21,66]. Through the use of the GLCM algorithm engrained within the GEE, contextual information for LULC mapping was added [22]. However, compared with previous works on OBIA, there are inconsistencies in terms of the most important texture metrics contributing to the classifications. For instance, the current study revealed that homogeneity attained the highest importance score of all the texture features. The result is not consistent with other studies [5,16] which, after investigating contrast, entropy, homogeneity, correlation, and mean, found contrast and entropy to be the most significant texture parameter at settlement level. Moreover, in an earlier study, Lai and Yang [67] utilized entropy to map layout of informal settlements and other land cover classes. In another study, Shekhar [68] found variance to be of high merit in the separation of built-up areas. Explaining differences in importance of various texture measures, the authors noted that the relevance of particular textural measures in capturing heterogeneity is reliant upon myriad factors, such as the image spatial resolution, fragmentation of the landscape under investigation, the between- or within-class differences among multifarious land cover categories, and the choice of appropriate textural features. For instance, in the context of variability in landscape components, Fallatah et al. [22] revealed that informal settlements in Jeddah differ in typology from informal settlements in Asia and Africa in that both settlement types are made up of similar building materials, causing textural complexities. On the other hand, in Pune, slums generally have diverse appearances that differ from planned residential complexes [17,69], whilst in Durban, they are usually made up of corrugated iron, plastics and wood, with some upgraded areas showing similarities to formal areas. Pratomo et al. [6] also indicated that such variability in morphology renders textural features' contribution context-specific and, sometimes, data-dependent.

Although high classification accuracies have been attained using OBIA methods within the GEE platform, there have been some uncertainties in the identification of informal settlements. From the confusion matrix (Table 4), there is evident misclassification between informal settlements and the "other urban" class. Whilst OBIA could accurately capture the spatial patterns of urban morphology, varying interurban morphological informal settlement features could explain the confusion [19]. Another cause could be the high density of backyard structures existing in some areas of the other "urban class". Evidencing this, Fallatah et al. [22] alluded to the complexity of urban areas because of their characteristic intermixing of diverse man-made and natural features, which may engender confusion between the object and its spectral reflectivity. According to Taubenböck et al. [7], a vital requirement in the delineation of informal settlements is the capability to identify small pockets of deprivation for informed decision-making. Although all LULC classes could be accurately captured in the current study, the approach failed to capture some discrete informal settlement patches. Figure 6 shows an informal settlement that is evident on high-resolution RGB imagery (Figure 6d, red rectangle), but missing on a classified image (Figure 6c, red rectangle).

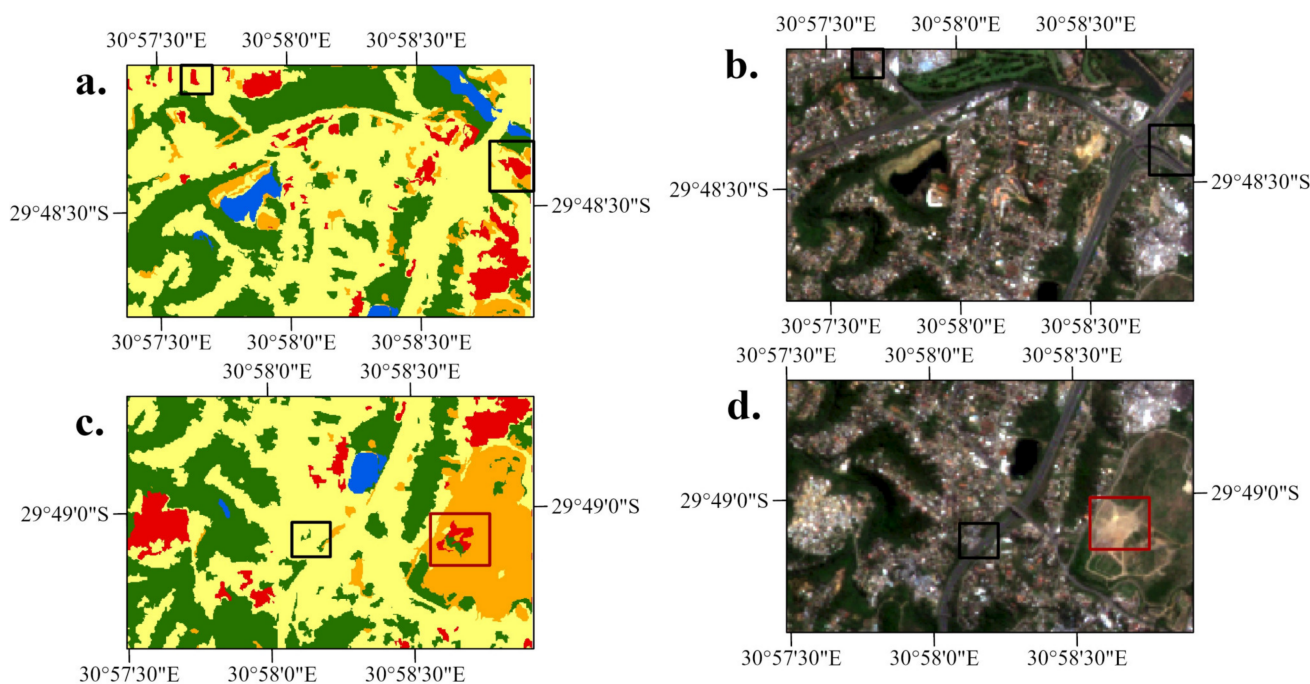


Figure 6. (a) shows misclassified informal settlement patches that on the ground (b) are commercial buildings. The red rectangles indicate misclassification of bare land (d) as informal settlement (c) (red patch). The black rectangle indicates missed informal settlement (c) that exists on the ground (d). The legend for (a,c) is included in Figure 3.

Such uncertainties can be explained in terms of complexity in defining the term informal settlement [6]. For instance, the same characteristic of density may differ locally depending on the developmental stages of the informal settlements, presenting inner-structural heterogeneity of these areas of deprivation [23]. Imprecisions may also be explained in terms of similarity in some morphological characteristics with formal built-up structures [18]. In the current study, there is evidence of other urban areas, for example, commercial buildings, being misrepresented as informal settlements (Figure 6a, black rectangle). The misclassification can be also explained in terms of the similarity of roofing materials, causing textural complexity. Evidently, confusion was also displayed between bare land and informal settlements. An informal settlement patch exists (Figure 6c, black rectangle) on an area that is predominantly bare (Figure 6d, black rectangle), which is evidence of potential similarity in spectrum [17]. Many informal settlements have corrugated iron roofs, and they may sometimes also have white backgrounds similar to bare ground, causing misclassification. Myint et al. [70] also notes that rusted iron sheets, that are also common as roofing materials in informal settlements, may tend to reflect similarly to bare soils which are usually reddish in colour, further contributing to misclassification.

Conceptual imprecision in OBIA within the GEE platform may also be compounded by complexity in application of segmentation algorithms in particular areas [31]. Hay Chung et al. [71] observed that, because of landscape heterogeneity, unvarying segmentation parameters may not yield the best results for all LULC types. Qu et al. [31] added that segmentation results may be compromised due to similarity in spectral characteristics among different land cover classes, as well as complexity in delineating the boundaries between the objects, especially between formal and informal areas. Some researchers [40,71] also noted that misclassifications could result from the quality of training samples that largely affects the performance of classifiers, resulting in failure to capture the dynamics. In that regard, Pratomo et al. [6] contend that it is critical to explicitly clarify the influence of these uncertainties on classification results when aiming at remote sensing-based informal settlement mapping.

Nevertheless, despite these limitations, the present study demonstrated the worth of classifying informal settlements using OBIA and multi-source data within GEE. However, GEE computational limitations can make OBIA application in large study areas difficult. The “export-to-asset” steps, based on background tasks, can help in OBIA applications in such areas.

5. Conclusions

This study presented an object-based approach for informal settlement identification within the GEE, using integrated datasets from PL, S2, and S1. GEE cloud computing was successfully applied for informal settlement mapping in Durban, South Africa. The GEE provided a powerful analysis platform for classification, allowing image segmentation and texture feature extraction using inbuilt SNIC and GLCM algorithms, respectively. The land cover classification yielded high overall accuracy (96%) and informal settlement identification accuracy of 87% (F-score). The derived error metrics presented reasonable agreement between the classified output with the ground truth statistics from Google Earth Pro. The informal settlement map indicated that a satisfactory outcome was achieved through the proposed object-based approach and could form the basis for deriving subsequent on-demand products.

The proposed approach presents opportunities for future research in monitoring the spatiotemporal dynamics of informal settlements over time. An understanding of informal settlement dynamics would assist in planning and fundamental decision-making for expediting informed management of cities.

Author Contributions: D.M. developed the aim and objective of the research and did conceptualization of manuscript, data and result analysis, as well original draft preparation. O.M., as the main supervisor, verified the analytical approaches and results of the study, including interpretation and discussion of the obtained results. M.N., as my co-supervisor, also constructively gave comments and suggestions that helped to improve the manuscript. M.V. contributed with Google Earth Engine scripting, helped with the methodology development, and editing of the manuscript. All authors have read and agreed to the published version of the manuscript.

Funding: This study was supported by the University of Kwa-Zulu Natal (UKZN) Big Data for Science and Society Project (BDSS). We also acknowledge SARChI Chair in Land Use Planning and Management, Grant no 84157 for their generous financial support.

Data Availability Statement: Sentinel-2 and Sentinel-1 data used in the research are available within Google Earth Engine (GEE). NICFI Planet data are accessible for the tropical area within GEE after NICFI (Norway’s International Climate and Forest Initiative) approval. The GEE codes developed in this research are available by emailing the author upon any reasonable request.

Acknowledgments: The Authors thank the NICFI (Norway’s International Climate and Forest Initiative) for having allowed the access to PlanetScope data within GEE.

Conflicts of Interest: The authors declare no conflict of interest.

References

1. Wurm, M.; Stark, T.; Zhu, X.X.; Weigand, M.; Taubenböck, H. Semantic segmentation of slums in satellite images using transfer learning on fully convolutional neural networks. *ISPRS J. Photogramm. Remote Sens.* **2019**, *150*, 59–69. [[CrossRef](#)]
2. Hofmann, P.; Taubenböck, H.; Werthmann, C. Monitoring and modelling of informal settlements-A review on recent developments and challenges. In Proceedings of the 2015 Joint Urban Remote Sensing Event (JURSE), Lausanne, Switzerland, 30 March–1 April 2015; pp. 1–4.
3. Kuffer, M.; Thomson, D.R.; Boo, G.; Mahabir, R.; Grippa, T.; Vanhuyse, S.; Engstrom, R.; Ndugwa, R.; Makau, J.; Darin, E.; et al. The Role of Earth Observation in an Integrated Deprived Area Mapping “System” for Low-to-Middle Income Countries. *Remote Sens.* **2020**, *12*, 982. [[CrossRef](#)]
4. UN-Habitat. *World Cities Report 2016: Urbanization and Development—Emerging Futures*; World Cities Report; UN: Nairobi, Kenya, 2016; ISBN 978-92-1-058281-0.
5. Fallatah, A.; Jones, S.; Wallace, L.; Mitchell, D. Combining Object-Based Machine Learning with Long-Term Time-Series Analysis for Informal Settlement Identification. *Remote Sens.* **2022**, *14*, 1226. [[CrossRef](#)]

6. Pratomo, J.; Kuffer, M.; Martinez, J.; Kohli, D. Coupling Uncertainties with Accuracy Assessment in Object-Based Slum Detections, Case Study: Jakarta, Indonesia. *Remote Sens.* **2017**, *9*, 1164. [[CrossRef](#)]
7. Taubenböck, H.; Kraff, N.J.; Wurm, M. The morphology of the Arrival City—A global categorization based on literature surveys and remotely sensed data. *Appl. Geogr.* **2018**, *92*, 150–167. [[CrossRef](#)]
8. Kraff, N.J.; Wurm, M.; Taubenböck, H. The dynamics of poor urban areas—Analyzing morphologic transformations across the globe using Earth observation data. *Cities* **2020**, *107*, 102905. [[CrossRef](#)]
9. Belenok, V.; Noszczyk, T.; Hebryn-Baidy, L.; Kryachok, S. Investigating anthropogenically transformed landscapes with remote sensing. *Remote Sens. Appl. Soc. Environ.* **2021**, *24*, 100635. [[CrossRef](#)]
10. Farda, N.M. Multi-temporal Land Use Mapping of Coastal Wetlands Area using Machine Learning in Google Earth Engine. *IOP Conf. Ser. Earth Environ. Sci.* **2017**, *98*, 012042. [[CrossRef](#)]
11. Wang, J.; Kuffer, M.; Roy, D.; Pfeffer, K. Deprivation pockets through the lens of convolutional neural networks. *Remote Sens. Environ.* **2019**, *234*, 111448. [[CrossRef](#)]
12. Kuffer, M.; Pfeffer, K.; Sliuzas, R.; Baud, I. Extraction of Slum Areas From VHR Imagery Using GLCM Variance. *IEEE J. Sel. Top. Appl. Earth Obs. Remote Sens.* **2016**, *9*, 1830–1840. [[CrossRef](#)]
13. Mboga, N.; Persello, C.; Bergado, J.; Stein, A. Detection of Informal Settlements from VHR Images Using Convolutional Neural Networks. *Remote Sens.* **2017**, *9*, 1106. [[CrossRef](#)]
14. Mudau, N.; Mhangara, P. Investigation of Informal Settlement Indicators in a Densely Populated Area Using Very High Spatial Resolution Satellite Imagery. *Sustainability* **2021**, *13*, 4735. [[CrossRef](#)]
15. Prabhu, R.; Parvathavarthini, B. An enhanced approach for informal settlement extraction from optical data using morphological profile-guided filters: A case study of Madurai city. *Int. J. Remote Sens.* **2021**, *42*, 6688–6705. [[CrossRef](#)]
16. Fallatah, A.; Jones, S.; Mitchell, D. Object-based random forest classification for informal settlements identification in the Middle East: Jeddah a case study. *Int. J. Remote Sens.* **2020**, *41*, 4421–4445. [[CrossRef](#)]
17. Kohli, D.; Sliuzas, R.; Stein, A. Urban slum detection using texture and spatial metrics derived from satellite imagery. *J. Spat. Sci.* **2016**, *61*, 405–426. [[CrossRef](#)]
18. Mugiraneza, T.; Nascetti, A.; Ban, Y. WorldView-2 Data for Hierarchical Object-Based Urban Land Cover Classification in Kigali: Integrating Rule-Based Approach with Urban Density and Greenness Indices. *Remote Sens.* **2019**, *11*, 2128. [[CrossRef](#)]
19. Stark, T.; Wurm, M.; Zhu, X.X.; Taubenböck, H. Satellite-Based Mapping of Urban Poverty with Transfer-Learned Slum Morphologies. *IEEE J. Sel. Top. Appl. Earth Obs. Remote Sens.* **2020**, *13*, 5251–5263. [[CrossRef](#)]
20. Leonita, G.; Kuffer, M.; Sliuzas, R.; Persello, C. Machine Learning-Based Slum Mapping in Support of Slum Upgrading Programs: The Case of Bandung City, Indonesia. *Remote Sens.* **2018**, *10*, 1522. [[CrossRef](#)]
21. Kohli, D.; Warwadekar, P.; Kerle, N.; Sliuzas, R.; Stein, A. Transferability of Object-Oriented Image Analysis Methods for Slum Identification. *Remote Sens.* **2013**, *5*, 4209–4228. [[CrossRef](#)]
22. Fallatah, A.; Jones, S.; Mitchell, D.; Kohli, D. Mapping informal settlement indicators using object-oriented analysis in the Middle East. *Int. J. Digit. Earth* **2019**, *12*, 802–824. [[CrossRef](#)]
23. Kohli, D.; Sliuzas, R.; Kerle, N.; Stein, A. An ontology of slums for image-based classification. *Comput. Environ. Urban Syst.* **2012**, *36*, 154–163. [[CrossRef](#)]
24. Phan, T.N.; Kuch, V.; Lehnert, L.W. Land Cover Classification using Google Earth Engine and Random Forest Classifier—The Role of Image Composition. *Remote Sens.* **2020**, *12*, 2411. [[CrossRef](#)]
25. Shafizadeh-Moghadam, H.; Khazaei, M.; Alavipanah, S.K.; Weng, Q. Google Earth Engine for large-scale land use and land cover mapping: An object-based classification approach using spectral, textural and topographical factors. *GISci. Remote Sens.* **2021**, *58*, 914–928. [[CrossRef](#)]
26. Teluguntla, P.; Thenkabail, P.S.; Oliphant, A.; Xiong, J.; Gumma, M.K.; Congalton, R.G.; Yadav, K.; Huete, A. A 30-m landsat-derived cropland extent product of Australia and China using random forest machine learning algorithm on Google Earth Engine cloud computing platform. *ISPRS J. Photogramm. Remote Sens.* **2018**, *144*, 325–340. [[CrossRef](#)]
27. Kelley, L.C.; Pitcher, L.; Bacon, C. Using Google Earth Engine to Map Complex Shade-Grown Coffee Landscapes in Northern Nicaragua. *Remote Sens.* **2018**, *10*, 952. [[CrossRef](#)]
28. Yang, G.; Yu, W.; Yao, X.; Zheng, H.; Cao, Q.; Zhu, Y.; Cao, W.; Cheng, T. AGTOC: A novel approach to winter wheat mapping by automatic generation of training samples and one-class classification on Google Earth Engine. *Int. J. Appl. Earth Obs. Geoinf.* **2021**, *102*, 102446. [[CrossRef](#)]
29. Achanta, R.; Susstrunk, S. Superpixels and polygons using simple non-iterative clustering. In Proceedings of the IEEE Conference on Computer Vision and Pattern Recognition (CVPR), Honolulu, HI, USA, 21–26 July 2017; pp. 4651–4660.
30. Luo, C.; Qi, B.; Liu, H.; Guo, D.; Lu, L.; Fu, Q.; Shao, Y. Using Time Series Sentinel-1 Images for Object-Oriented Crop Classification in Google Earth Engine. *Remote Sens.* **2021**, *13*, 561. [[CrossRef](#)]
31. Qu, L.a.; Chen, Z.; Li, M.; Zhi, J.; Wang, H. Accuracy Improvements to Pixel-Based and Object-Based LULC Classification with Auxiliary Datasets from Google Earth Engine. *Remote Sens.* **2021**, *13*, 453. [[CrossRef](#)]
32. Vizzari, M. PlanetScope, Sentinel-2, and Sentinel-1 Data Integration for Object-Based Land Cover Classification in Google Earth Engine. *Remote Sens.* **2022**, *14*, 2628. [[CrossRef](#)]
33. Tassi, A.; Gigante, D.; Modica, G.; Di Martino, L.; Vizzari, M. Pixel- vs. Object-Based Landsat 8 Data Classification in Google Earth Engine Using Random Forest: The Case Study of Maiella National Park. *Remote Sens.* **2021**, *13*, 2299. [[CrossRef](#)]

34. Tassi, A.; Vizzari, M. Object-Oriented LULC Classification in Google Earth Engine Combining SNIC, GLCM, and Machine Learning Algorithms. *Remote Sens.* **2020**, *12*, 3776. [[CrossRef](#)]
35. Hall-Beyer, M. Practical guidelines for choosing GLCM textures to use in landscape classification tasks over a range of moderate spatial scales. *Int. J. Remote Sens.* **2017**, *38*, 1312–1338. [[CrossRef](#)]
36. Zhang, K.; Dong, X.; Liu, Z.; Gao, W.; Hu, Z.; Wu, G. Mapping Tidal Flats with Landsat 8 Images and Google Earth Engine: A Case Study of the China's Eastern Coastal Zone circa 2015. *Remote Sens.* **2019**, *11*, 924. [[CrossRef](#)]
37. Li, M.; Zhang, R.; Luo, H.; Gu, S.; Qin, Z. Crop Mapping in the Sanjiang Plain Using an Improved Object-Oriented Method Based on Google Earth Engine and Combined Growth Period Attributes. *Remote Sens.* **2022**, *14*, 273. [[CrossRef](#)]
38. Mahdianpari, M.; Salehi, B.; Rezaee, M.; Mohammadimanesh, F.; Zhang, Y. Very Deep Convolutional Neural Networks for Complex Land Cover Mapping Using Multispectral Remote Sensing Imagery. *Remote Sens.* **2018**, *10*, 1119. [[CrossRef](#)]
39. Mahdianpari, M.; Salehi, B.; Mohammadimanesh, F.; Brisco, B. An Assessment of Simulated Compact Polarimetric SAR Data for Wetland Classification Using Random Forest Algorithm. *Can. J. Remote Sens.* **2017**, *43*, 468–484. [[CrossRef](#)]
40. Amani, M.; Brisco, B.; Afshar, M.; Mirmazloumi, S.M.; Mahdavi, S.; Mirzadeh, S.M.J.; Huang, W.; Granger, J. A generalized supervised classification scheme to produce provincial wetland inventory maps: An application of Google Earth Engine for big geo data processing. *Big Earth Data* **2019**, *3*, 378–394. [[CrossRef](#)]
41. Mahdianpari, M.; Salehi, B.; Mohammadimanesh, F.; Homayouni, S.; Gill, E. The First Wetland Inventory Map of Newfoundland at a Spatial Resolution of 10 m Using Sentinel-1 and Sentinel-2 Data on the Google Earth Engine Cloud Computing Platform. *Remote Sens.* **2018**, *11*, 43. [[CrossRef](#)]
42. Tavares, P.A.; Beltrao, N.E.S.; Guimaraes, U.S.; Teodoro, A.C. Integration of Sentinel-1 and Sentinel-2 for Classification and LULC Mapping in the Urban Area of Belem, Eastern Brazilian Amazon. *Sensors* **2019**, *19*, 1140. [[CrossRef](#)]
43. Rao, P.; Zhou, W.; Bhattarai, N.; Srivastava, A.K.; Singh, B.; Poonia, S.; Lobell, D.B.; Jain, M. Using Sentinel-1, Sentinel-2, and Planet Imagery to Map Crop Type of Smallholder Farms. *Remote Sens.* **2021**, *13*, 1870. [[CrossRef](#)]
44. Bwangoy, J.-R.B.; Hansen, M.C.; Roy, D.P.; Grandi, G.D.; Justice, C.O. Wetland mapping in the Congo Basin using optical and radar remotely sensed data and derived topographical indices. *Remote Sens. Environ.* **2010**, *114*, 73–86. [[CrossRef](#)]
45. Liu, H.; Xiao, P.; Zhang, X.; Zhou, X.; Li, J.; Guo, R. Object-based island green cover mapping by integrating UAV multispectral image and LiDAR data. *J. Appl. Remote Sens.* **2021**, *15*, 034512. [[CrossRef](#)]
46. Williams, D.; Mánuez Costa, M.; Celliers, L.; Sutherland, C. Informal Settlements and Flooding: Identifying Strengths and Weaknesses in Local Governance for Water Management. *Water* **2018**, *10*, 871. [[CrossRef](#)]
47. Marx, C.; Charlton, S. *Global Report on Human Settlements*; UN-HABITAT (Hg.): Durban, South Africa, 2003; pp. 195–223.
48. Matarira, D.; Mutanga, O.; Naidu, M. Google Earth Engine for Informal Settlement Mapping: A Random Forest Classification Using Spectral and Textural Information. *Remote Sens.* **2022**, *14*, 5130. [[CrossRef](#)]
49. Marfai, M.A.; Farda, N.M.; Khakhim, N.; Wicaksono, P.; Wicaksono, A. Tidal Correction Effects Analysis on Shoreline Mapping in Jepara Regency. *J. Appl. Geospat. Inf.* **2018**, *2*, 145–151. [[CrossRef](#)]
50. Carrasco, L.; O'Neil, A.; Morton, R.; Rowland, C. Evaluating Combinations of Temporally Aggregated Sentinel-1, Sentinel-2 and Landsat 8 for Land Cover Mapping with Google Earth Engine. *Remote Sens.* **2019**, *11*, 288. [[CrossRef](#)]
51. Abebe, M.S.; Derebew, K.T.; Gemedo, D.O. Exploiting temporal-spatial patterns of informal settlements using GIS and remote sensing technique: A case study of Jimma city, Southwestern Ethiopia. *Environ. Syst. Res.* **2019**, *8*, 6. [[CrossRef](#)]
52. Bouzekri, S.; Lasbet, A.A.; Lachehab, A. A New Spectral Index for Extraction of Built-Up Area Using Landsat-8 Data. *J. Indian Soc. Remote Sens.* **2015**, *43*, 867–873. [[CrossRef](#)]
53. Diek, S.; Fornallaz, F.; Schaeppman, M.E. Barest Pixel Composite for Agricultural Areas Using Landsat Time Series. *Remote Sens.* **2017**, *9*, 1245. [[CrossRef](#)]
54. Nguyen, H.T.T.; Doan, T.M.; Tomppo, E.; McRoberts, R.E. Land Use/Land Cover Mapping Using Multitemporal Sentinel-2 Imagery and Four Classification Methods—A Case Study from Dak Nong, Vietnam. *Remote Sens.* **2020**, *12*, 1367. [[CrossRef](#)]
55. Vergni, L.; Vinci, A.; Todisco, F.; Santaga, F.S.; Vizzari, M. Comparing Sentinel-1, Sentinel-2, and Landsat-8 data in the early recognition of irrigated areas in central Italy. *J. Agric. Eng.* **2021**, *52*. [[CrossRef](#)]
56. Hu, T.; Liu, J.; Zheng, G.; Li, Y.; Xie, B. Quantitative assessment of urban wetland dynamics using high spatial resolution satellite imagery between 2000 and 2013. *Sci Rep* **2018**, *8*, 7409. [[CrossRef](#)]
57. Achanta, R.; Shaji, A.; Smith, K.; Lucchi, A.; Fua, P.; Süsstrunk, S. SLIC superpixels compared to state-of-the-art superpixel methods. *IEEE Trans. Pattern Anal. Mach. Intell.* **2012**, *34*, 2274–2282. [[CrossRef](#)]
58. Chen, Y.; Zhou, Y.n.; Ge, Y.; An, R.; Chen, Y. Enhancing Land Cover Mapping through Integration of Pixel-Based and Object-Based Classifications from Remotely Sensed Imagery. *Remote Sens.* **2018**, *10*, 77. [[CrossRef](#)]
59. Prabhu, R.; Alagu Raja, R.A. Urban Slum Detection Approaches from High-Resolution Satellite Data Using Statistical and Spectral Based Approaches. *J. Indian Soc. Remote Sens.* **2018**, *46*, 2033–2044. [[CrossRef](#)]
60. Wurm, M.; Taubenböck, H.; Weigand, M.; Schmitt, A. Slum mapping in polarimetric SAR data using spatial features. *Remote Sens. Environ.* **2017**, *194*, 190–204. [[CrossRef](#)]
61. Zurqani, H.A.; Post, C.J.; Mikhailova, E.A.; Allen, J.S. Mapping Urbanization Trends in a Forested Landscape Using Google Earth Engine. *Remote Sens. Earth Syst. Sci.* **2019**, *2*, 173–182. [[CrossRef](#)]
62. Malambo, L.; Heatwole, C.D. Automated training sample definition for seasonal burned area mapping. *ISPRS J. Photogramm. Remote Sens.* **2020**, *160*, 107–123. [[CrossRef](#)]

63. Zhao, Y.; Zhu, W.; Wei, P.; Fang, P.; Zhang, X.; Yan, N.; Liu, W.; Zhao, H.; Wu, Q. Classification of Zambian grasslands using random forest feature importance selection during the optimal phenological period. *Ecol. Indic.* **2022**, *135*, 108529. [[CrossRef](#)]
64. Kpienbaareh, D.; Sun, X.; Wang, J.; Luginaah, I.; Bezner Kerr, R.; Lupafya, E.; Dakishoni, L. Crop Type and Land Cover Mapping in Northern Malawi Using the Integration of Sentinel-1, Sentinel-2, and PlanetScope Satellite Data. *Remote Sens.* **2021**, *13*, 700. [[CrossRef](#)]
65. Hamud, A.M.; Shafri, H.Z.M.; Shaharun, N.S.N. Monitoring Urban Expansion and Land Use/ Land cover Changes in Banadir, Somalia, using Google Earth Engine (GEE). *IOP Conf. Ser. Earth Environ. Sci.* **2021**, *767*, 012041. [[CrossRef](#)]
66. Duque, J.C.; Patino, J.E.; Ruiz, L.A.; Pardo-Pascual, J.E. Measuring intra-urban poverty using land cover and texture metrics derived from remote sensing data. *Landsc. Urban Plan.* **2015**, *135*, 11–21. [[CrossRef](#)]
67. Lai, F.; Yang, X. Integrating spectral and non-spectral data to improve urban settlement mapping in a large Latin-American city. *GISci. Remote Sens.* **2020**, *57*, 830–844. [[CrossRef](#)]
68. Shekhar, S. Detecting slums from Quick Bird data in Pune using an object oriented approach. *Int. Arch. Photogramm. Remote Sens. Spat. Inf. Sci.* **2012**, *39*, 519–524. [[CrossRef](#)]
69. Gevaert, C.M.; Persello, C.; Sliuzas, R.; Vosselman, G. Classification of Informal Settlements through the Integration of 2d and 3d Features Extracted from Uav Data. *ISPRS Ann. Photogramm. Remote Sens. Spat. Inf. Sci.* **2016**, *III-3*, 317–324. [[CrossRef](#)]
70. Myint, S.W.; Gober, P.; Brazel, A.; Grossman-Clarke, S.; Weng, Q. Per-pixel vs. object-based classification of urban land cover extraction using high spatial resolution imagery. *Remote Sens. Environ.* **2011**, *115*, 1145–1161. [[CrossRef](#)]
71. Hay Chung, L.C.; Xie, J.; Ren, C. Improved machine-learning mapping of local climate zones in metropolitan areas using composite Earth observation data in Google Earth Engine. *Build. Environ.* **2021**, *199*, 107879. [[CrossRef](#)]

Disclaimer/Publisher’s Note: The statements, opinions and data contained in all publications are solely those of the individual author(s) and contributor(s) and not of MDPI and/or the editor(s). MDPI and/or the editor(s) disclaim responsibility for any injury to people or property resulting from any ideas, methods, instructions or products referred to in the content.